Development and Optical Characterization of Supersonic Gas Targets for High-Intensity Laser Plasma Studies

Ricardo E. Samad
IPEN-CNEN/SP
São Paulo, Brazil
resamad@gmail.com

Armando V. F. Zuffi
IPEN-CNEN/SP
São Paulo, Brazil
armandozuffi@gmail.com

Edison P. Maldonado
IEE-ITA
São José dos Campos, Brazil
puigmald@gmail.com

Nilson D. Vieira Junior
IPEN-CNEN/SP
São Paulo, Brazil
nilsondiasvieirajr@gmail.com

***Abstract*—Laser particle acceleration is a rapid growing field due to the compactness and smaller cost when compared to traditional accelerators, as well as the potential for new applications resulting from the unique characteristics of the beams generated. Frequently, laser acceleration techniques require laser intensities higher than 100's of PW/cm^2 and high-density gas targets, with specific profiles. In the effort to implement laser electron acceleration in our laboratories, we report the development of submillimetric, supersonic gas nozzles, the implementation of optical techniques for the determination of the gas jets density profiles, and the characterization of laser-induced plasmas obtained at laser intensities surpassing 10^{16} W/cm^2. The characterization techniques employed include plasma spectroscopy, interferograms and Schlieren images.**

Keywords—Laser Plasma, Ultrashort Pulses, Optical Characterization, Laser Electron Acceleration

I. INTRODUCTION

Laser plasma particle accelerators were proposed almost 40 years ago by Tajima and Dawson [1], and nowadays high energy electron and protons beams are generated from table-top laser systems [2, 3]. This new technology is expected to allow cheaper and more compact accelerators, with high temporal resolution and other new features for many present and future applications [4-6]. Different operating physical regimes and systems exist, but the underlying requirement for laser acceleration is the use of tens of femtoseconds ultrashort pulses focused to intensities above 10^{17} W/cm^2 over a few millimeters. Those conditions are used to excite a plasma wakefield behind the laser pulse, which can be used to accelerate electrons [7]. This plasma wave carries the electrons and can sustain electric fields higher than 100 GV/m, well above the 100 MV/m typically found in conventional RF accelerators.

In laser wakefield electron accelerators, beams composed by ultrafast burst of electrons (bunches) can be obtained with energies typically ranging from MeV to GeV, with a few percent energy dispersion, divergence under 1 mrad, electric charge on the 10-100 pC range and duration as short as 1 fs [5, 8], 3 orders of magnitude shorter than those obtainable in synchrotrons.

The interaction of these beams with matter allows the development of tunable, compact sources of high energy ionizing radiation [9], which are already being used in new imaging techniques [10]. Other researched applications of laser particle accelerators are the production of isotopes for medicine [11, 12], protontherapy, hadron therapy [6, 13] and fast ignition in fusion targets [14, 15].

To accelerate electrons using ultrashort pulses, gas targets are generally used [16], in which a plasma is generated by laser-induced ionization for intensities above 10^{14} W/cm^2. Those intensities must occur in the leading edge of the laser pulse, and the interaction of the remaining part of the pulse with the generated plasma is possible only below a limiting density of plasma electrons, the so-called critical density, n_{cr}, specific for each laser frequency. For the Ti:Sapphire wavelength, 785 nm, the critical density is $n_{cr} = 1.8 \times 10^{21}$ cm^{-3} [17, 18]. Typically, in this generated underdense plasma, the laser pulse propagates without high losses, displacing the charges by the ponderomotive force and exciting an intense plasma wave in its wakefield [16, 19].

The technology of gas targets for laser-plasma studies is mainly composed of nozzles, ducts and cells. Gas nozzles are simple and versatile devices to create reproducible high-density, sonic and supersonic gas targets for laser-plasma experiments. A cylindrical nozzle geometry generates a sonic flow into a lower pressure chamber, while a conical divergent nozzle produces a supersonic flow with a Mach number dependent on the nozzle geometric details. For gas jets with high Mach numbers, sharp jet-vacuum boundaries and flat-top gas density profiles are typically obtained, characteristics that can enhance the laser interaction, simplifying the design and analysis of laser-plasma experiments [6]. High-intensity laser experiments currently using such gas nozzles involve laser frequency upshift and high-harmonic generation, laser filamentation, relativistic self-focusing, laser-driven electron acceleration, THz generation, extreme ultraviolet and x-ray beam generation, laser pulse compression, among others [20].

Gas jets with submillimetric thicknesses and peak density from 10^{18} to 10^{21} atoms/cm^3 allow the generation of highly nonlinear waves of plasma, even for mJ-class laser pulses, which require tightly focused beams [21]. When using sonic and low Mach number flows, the laser should be focused in the region close to the exit of the nozzle, since the gas density quickly drops when moving away from it. On the other hand, for high Mach nozzles, the jet is highly collimated, keeping the density profile almost constant for a long extension from the nozzle exit, but with much lower values compared to the sonic one.

In our laboratory we are working to implement a laser electron acceleration infrastructure, and the first step is to create controlled gas targets and focus the laser beam to small spots. For this, we are fabricating nozzles and developing and implementing gas jet and plasma characterization techniques. Here we report our first results of the gas jet characterization by Schlieren shadowgraphy and interferometry [22], the beam focusing and plasma spectroscopy.

This work was supported by FAPESP and CNPq grants.

978-1-5386-6702-6/18/$31.00 ©2018 IEEE

II. Implementing Gas Targets for Laser-Plasma

A. Nozzle Design

Fig. 1 exhibits a sketch of a convergent-divergent nozzle, known as de Laval nozzle [20]. This kind of nozzle is a duct that contains a region of constriction (a throat, like a Venturi tube) and an expanding exit section that accelerates a pressurized gas by converting its heat into kinetic energy. Two limiting cases exist: the sonic nozzle, in which the throat and the exit radii are approximately the same, and the supersonic nozzle, in which the throat radius is smaller than that of the exit. In both geometries the flow is always sonic (or choked) at the throat section and the acceleration occurs at the exit duct. A nozzle will only choke at the throat if the pressure difference between the chambers is enough to produce sonic speeds by mass flow through the nozzle, otherwise no supersonic flow is achieved. The minimum pressure ratio for the choked flow to occur varies with the gas type but is typically around 0.53 (for N_2).

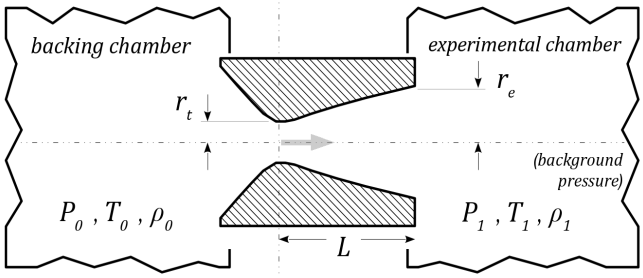

Fig. 1. Sketch of a de Laval nozzle. The throat radius is r_t, the exit radius r_e, and L is the length of the conical exit section. P, T and ρ are the gas pressure, temperature and density, respectively.

The sonic regime, in which the Mach number is $M \approx 1$, is characterized by high gas densities at the nozzle exit that quickly drop with distance, with a bell-shaped density profile. The highly supersonic regime, $M >> 1$, presents a collimated gas jet with a flat density profile. The optimal M is thus determined by the kind of experiment, its objectives, the available laser parameters such as peak power and focused beam area and the available gas equipment that defines the operational backing pressure.

A quasi-1D model of a de Laval nozzle, assuming isentropic flow, leads to very useful expressions for the mass flow rate, $\dot{m}$, (1), Mach number as a function of the exit to throat area ratio, A_e/A_t, (2), divergence angle for vacuum-quality background pressure, α, (3) and maximum jet gas density, ρ, (4) (typically a good prediction for the gas jet in the immediate vicinity from the nozzle exit, at its symmetry axis) [21]:

$$\dot{m} = A_t P_0 \sqrt{\frac{\gamma}{R T_0}} \left(\frac{2}{\gamma+1} \right)^{\frac{\gamma+1}{2(\gamma-1)}} \quad (1)$$

$$\frac{A_e}{A_t} = \frac{1}{M} \left[\frac{2+(\gamma-1)M^2}{\gamma+1} \right]^{\frac{\gamma+1}{2(\gamma-1)}} \quad (2)$$

$$\alpha = 1/M \quad (3)$$

$$\frac{\rho}{\rho_0} = \frac{1}{M} \left[\frac{\gamma+1}{2+(\gamma-1)M^2} \right]^{\frac{1}{(\gamma-1)}}, \quad (4)$$

where P_0, T_0, ρ_0 and P_1, T_1, ρ_1 are reservoir gas pressure, temperature and density for the backing and experimental chambers, respectively; γ is the heat capacity ratio, or adiabatic index (~7/5 for N_2) and R is the specific gas constant (297 J/kg·K for N_2). Once the thermodynamic parameters are defined (when the gas is chosen) and the ratio between the throat and the exit is specified, the Mach number and the flow parameters are fixed. This model disregards the exact value of the background density, ρ_1, the presence of shock waves in the downstream flow, as well as the nozzle length, (L) and other geometrical features like the length of the converging region, shapes and curvatures, all these affecting the jet discharge and speed (and pressure) as second-order corrections.

Using this simple model, we designed a Mach 2.5 nozzle to generate a 250 µm-thick, continuous N_2 jet flow in a vacuum chamber. We manufactured the nozzle in our laboratory, using a homemade ultrafast laser machining system to etch a conic-shaped hole on a 500 µm-thick wall on the surface of a ¼" diameter copper rod, drilled with an eccentric hollow duct, as shown in Fig. 2. This "eccentric pipe section" is open on one end and closed on the other to withstand the internal pressure, which reaches several bars, working as a gas line termination element. The nozzle etching was precisely performed by trepanation using 200 µJ, 30 fs laser pulses at 4 kHz, a 25 cm focusing achromatic doublet, and a computer controlled 3-axis positioning system. The nozzle exit diameter is approximately 250 µm (measured by a Zegage optical profiler, Zygo Corp.) and the inner hole diameter is approximately 150 µm, as required for a M ≈ 2.5 supersonic nozzle.

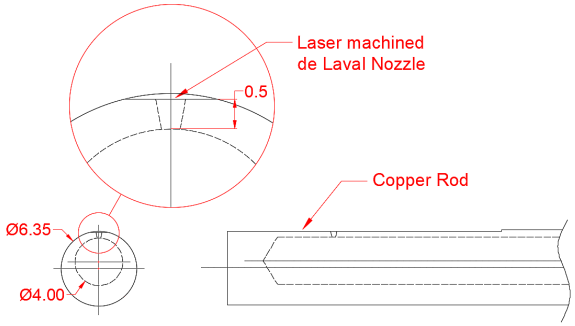

Fig. 2. Submillimetric de Laval nozzle, laser-machined in a copper rod. All dimensions in mm.

Assuming a N_2 backing pressure of 15 bar and using (1) to (4), we expected to obtain the mass ($\dot{m}$) and flow (v_1) rates, number density (n) and angle (α) shown in Table I, where n_0 is the atomic number density in the backing chamber.

TABLE I. Calculated Characteristics for the Manufactured Nozzle, Mach 2.5.

$\dot{m}$ (kg/s)	v_1 (m^3/h)	n (cm^{-3})	n_0/n	α (deg)
6×10^{-5}	19.0	6×10^{19}	12	23.6

B. Gas Profile Measurement

To characterize the gas jet, we used two techniques: the Schlieren imaging (an enhanced variation of shadowgraphy) [23, 24] and the Mach–Zehnder interferometry, with the setup shown in Fig. 3: a polarized

633 nm He-Ne continuous beam is spatially filtered using a 30 µm pinhole and collimated to a 1 cm radius; the beam is split in a conventional Mach-Zehnder interferometer and passes through the gas jet in one arm; a 10 cm convergent lens positioned in the final optical axis, 12 cm away from the gas jet, produces a 5× magnified image of the jet at the CCD surface. To produce a Schlieren image, the interferometer arm without the gas jet is blocked (to eliminate the interference fringes), and a knife-edge is inserted at the focal point of the lens, where the He-Ne beam converges to a focus, and adjusted to maximize the contrast.

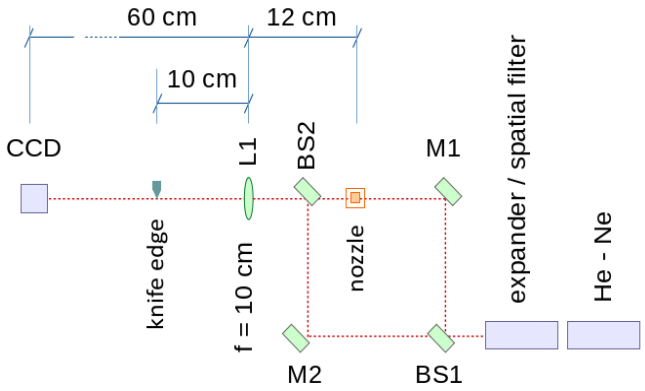

Fig. 3. Setup for the measurement of the gas jet profile and its density through Schlieren imaging and Mach–Zehnder interferometry, respectively.

We have also implemented a small vacuum chamber, with windows at the Brewster angle, which can be fitted to the cylindrical nozzle. With this chamber we have studied the nozzle performance when applying a backing pressure between 10 and 20 bar and the emerging gas jet flowing into two background pressures: 1 atm and ~10 mbar. Using the Schlieren technique we could easily identify the gas jet position, shape and size in the shadowgrams shown in Fig. 4. These images show the gas flow out of the nozzle into a) 1 atm background, and b) 10 mbar background. In both cases, the flow width at the nozzle exit (lower part of images) is around 200 µm. In the low-pressure environment, the underexpanded jet widens transversally and its density drops. In the 1 atm environment, nodes can be observed, where the overexpanded supersonic jet shockwaves converge into high density regions.

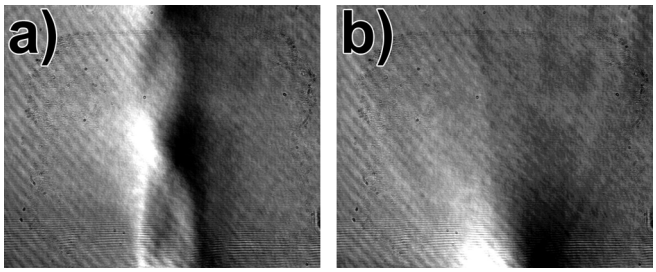

Fig. 4. Typical Schlieren image of the gas flow near the exit of our Mach 2.5 nozzle, in background pressures of a) 1 atm and b) 10 mbar. The nozzle exit is in the lower edge of the frame, and both images cover the first 750 µm of the jet; the applied backing pressure was 15 bars.

By analyzing interferograms like those from Fig. 5, which correspond to the shadowgrams shown in Fig. 4, the positions of maximum phase shift and the corresponding maximum local pressures attained are promptly recognized. For the 1 atm-background flow, Fig. 5a, a phase shift of $\Delta\varphi \approx 2\pi/6$ at ~300 µm above the nozzle exit is observed, corresponding to the node in Fig. 4a. This phase shift corresponds to a change in optical length of 106 nm. Assuming a flat profile for the 200 µm wide gas jet, the refraction index change is 5.0×10^{-4}, which for N_2 corresponds to 2 atm above the background, thus an absolute value of approximately 3 atm [25]. For the 10 mbar-background flow, Fig. 5b, a phase shift of $\Delta\varphi \approx 2\pi/5$ is observed immediately after the nozzle exit, corresponding to a change in optical length of 130 nm. Assuming a flat profile for the 200 µm wide gas jet, the change in refraction index is 6.5×10^{-4}, which for N_2 corresponds ~2 atm above the background. In this setup that is the approximate absolute value, corresponding to an atomic density of $\sim1\times10^{20}$ cm^3 [26].

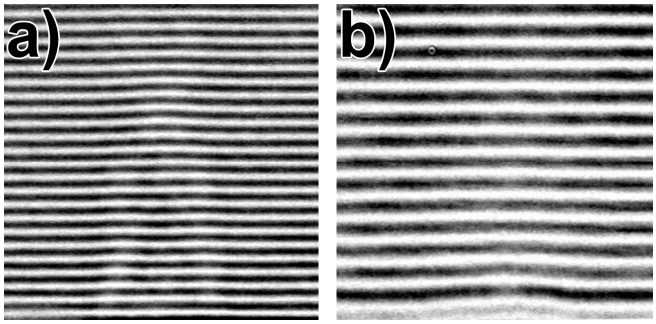

Fig. 5. Typical Mach-Zehnder interferograms for 633 nm HeNe continuous beam transmission through the cross section of the gas jet near the exit of our Mach 2.5 nozzle, in background pressures of a) 1 atm and b) 10 mbar. The nozzle exit is in the lower edge of the frame and both images cover the first 500 µm of the jet; the applied backing gas pressure was 15 bars.

III. Experimental Laser-Plasma Characteristics

C. *Laser Parameters*

To create a plasma in the gas jet, pulses from a Ti:Sapphire CPA laser system (Femtopower Compact Pro HR/HP, from Femtolasers) were used. This system generates 25 fs (FWHM) pulses centered at 785 nm, with 350 µJ of energy, in a 4 kHz repetition rate train of pulses, in a beam with $M^2 \approx 1.2$.

To focus the 14 GW pulses on the gas jet target, the laser beam was expanded and collimated to a beam with ~2 cm in diameter and focused by a 90° off-axis parabolic mirror, with 2.54 cm aperture and 5 cm focusing distance. To properly analyze the beam focus, a 10× magnification imaging optics was implemented using a 5 cm focal length doublet. The image of the beam at its waist was used to adjust the beam injection angle on the mirror and minimize the astigmatism. Fig. 6 presents the CCD image at the focus, showing a beamwaist of 4 µm, near the diffraction limit, with a 115 µm confocal parameter smaller than the gas jet width. Due to the asymmetry observed in the beam, which requires an adaptative optics system to be corrected, the waist encompasses 75% of the beam energy, generating 2.1×10^{16} W/cm^2 of intensity at this spot. We routinely obtain spots with this size and plan to insert a deformable mirror before the parabolic mirror, aiming to decrease the beamwaist and increase the amount of energy contained in it.

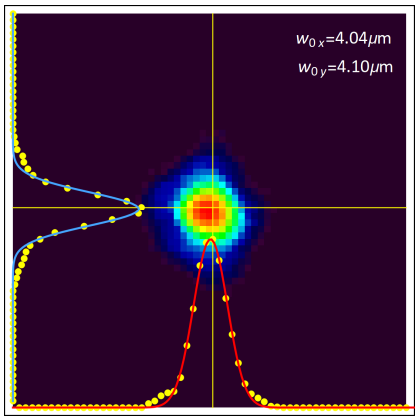

Fig. 6. High-intensity beam profile at the parabolic mirror focus.

D. *Plasma Characterization*

Switching off the HeNe laser (Fig. 3) allows the use of the same setup to magnify the plasma glow by using the lens-produced image on the CCD, registering its position and size. Fig. 7 shows the $1/e^2$ horizontal and vertical widths of the plasma obtained at various distances from the nozzle exit, using the gas jet in a 1 atm background pressure. The widths at ~350, ~750 and ~1250 µm from the nozzle were measured at the jet nodes (high density regions), while the others were measured at anti-nodes (low density) positions. The plasma length (horizontal) at the nodes are shorter than at the anti-nodes positions, a consequence of the denser plasmas formed that concentrate more energy absorbed from the laser pulses; also, the plasma length exhibits a tendency to grow as the distance from the nozzle exit increases since the consecutive nodes have smaller density than the previous ones. This tendency is not so clearly observed in the transversal (vertical) dimension of the plasma.

At the currently available laser peak power in the kHz regime, we have not observed any relativistic self-focusing effect. Besides, for this power level and experimental setup, no ionization-induced defocusing effects were detected.

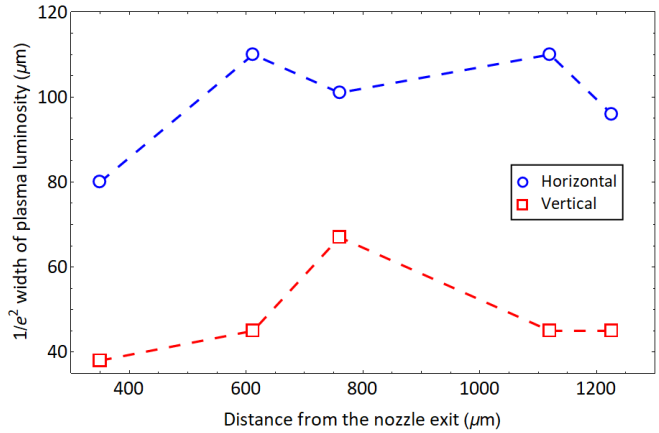

Fig. 7. Measurement data for the dimensions of the emissions from the laser-generated plasma (and plume) as function of the distance from nozzle exit, using the gas jet in 1 atm background.

Fig. 8 exhibits a composite picture of a Schlieren image of the gas jet and a plasma image. The laser is coming from the right, positioned to maximize the plasma emission. It can be seen that the plasma is created in the first half of the jet and has a length of ~100 µm, compatible with the beam confocal length.

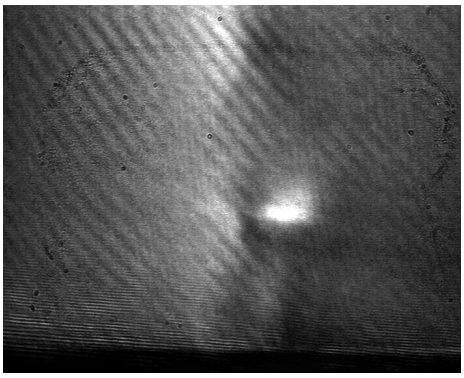

Fig. 8. Superposition of the Schlieren and plasma images, showing where typically the plasma forms. The laser pulses came from the right.

The plasma ionization state can be obtained by measuring its emission spectrum, which has two main components. The first one is its blackbody emission, and the other is composed by its atomic emission lines, that immediately provide the ionization state. To perform this measurement, the plasma emission was collected by a telescope made with fused silica lenses, injected into an UV optical fiber and sent to an ECCD Echelle gated spectrometer (Aryelle-Butterfly, LTB). This gated spectrometer is used to eliminate the blackbody emission, that evanesces in hundreds of ns (for excitation with fs pulses) [27, 28], and provides an atomic emission spectrum with minimized background. Fig. 9 shows emission lines measured with a 50 ns gate, starting 50 and 80 ns after the laser pulse. The first spectrum shows 2 emission lines (414.343 nm and 415.148 nm) for the neutral Nitrogen (N I), and it can be seen that the background (blackbody emission) decreases for the spectrum measured 80 ns after the laser pulse, but do not fade completely. It is also seen that the spectra have a lot of noise that can mask the emission lines. In the lower graph, the 50 ns delayed spectrum clearly shows an emission line at 405.776 nm from the N^{3+} ion (N IV), which almost disappears on the 80 ns spectrum due to its 15 ns lifetime [29]. We could not detect higher ionization states, although the theory predicts [30] that, at the intensities obtained at the focus, N^{4+} should have been produced.

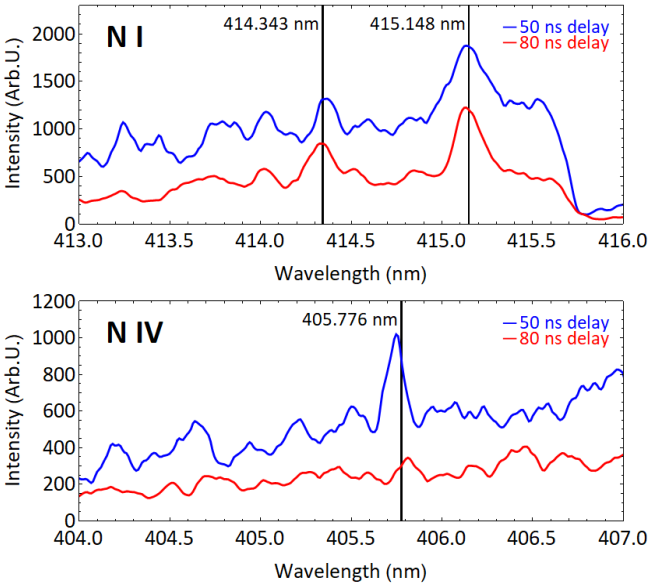

Fig. 9. Atomic emission spectra from the Nitrogen plasma at 50 and 80 ns after the laser pulse, for neutral and 3^+ nitrogen.

IV. Discussion and Conclusions

The observed gas jet flowing in a low-pressure chamber exhibits a 27° divergence angle (half angle from normal). The corresponding Mach number, retrieved from the model, would be for this case M=2.2 instead of the predicted 2.5 when designing the nozzle.

The foreseen volumetric rate for the designed nozzle operating at 15 bar backing pressure is 19 m^3/h. The used vacuum pump, Edwards model E2M18, has a maximum swept volume rate of 18 m^3/h and a nominal ultimate vacuum (total pressure) 0.2 mbar with gas ballast. Since our equilibrium background pressure was around 10 mbar, we infer that a higher-than-expected volume flow rate occurred (not measured). The same kind of disagreement was observed when measuring the in-vacuum supersonic jet pressure: a maximum of 2 atm, while the expected value when applying 15 bars was 1.2 atm. We consider that the higher values deviations of pressure and volume rate, as well as the observed lower Mach number, may be attributed to partial failure of the quasi-one-dimensional model for the microscopic supersonic nozzle due to influence of the non-considered geometrical factors such as length of the conical exit section, as well as wall-proximity effects [20].

Although we need to improve the signal to noise ratio on the atomic emission spectra measurements, we could measure ionization states up to N^{3+}. The expected electron density corresponding to these ionizations, together with the laser intensity obtained (>$2\cdot10^{16}$ W/cm^2), indicate that our experimental conditions should be close to obtaining the relativistic self-focusing, a condition known act as a trigger to the electron acceleration regime, mostly for low energy laser pulses [18].

Acknowledgments

We would like the thank Prof. Sudeep Banerjee of University of Nebraska, Lincoln, for helpful discussions. E. P. M. thanks the CNEN/CNPq Institutional Capacitation program, and A. V. F. Z. thanks CNPq for the scholarship.

References

[1] Tajima, T., and Dawson, J.M., "Laser Electron Accelerator," Phys. Rev. Lett., 43, pp. 267-270, 1979.

[2] Feister, S., "Relativistic electron acceleration by mJ-class kHz lasers normally incident on liquid targets," Opt. Expr., 25, pp. 18736-18750, 2017.

[3] Morrison, J.T., "MeV proton acceleration at kHz repetition rate from ultra-intense laser liquid interaction," New J. Phys., 20, pp. 9, 2018.

[4] Tajima, T., Nakajima, K., and Mourou, G., "Laser acceleration," Riv. Nuovo Cimento, 40, pp. 33-133, 2017.

[5] Malka, V., "Laser Plasma Accelerators," in Laser-Plasma Interactions and Applications, McKenna, P., Neely, D., Bingham, R. and Jaroszynski, D. Eds. Heidelberg: Springer, 2013, pp. 281-301.

[6] Giulietti, A., Laser-Driven Particle Acceleration Towards Radiobiology and Medicine, Springer International Publishing, 2016, pp. 320.

[7] Leemans, W.P., "Laser-driven plasma-based accelerators: Wakefield excitation, channel guiding, and laser triggered particle injection," Phys. Plasmas, 5, pp. 1615-1623, 1998.

[8] Gustas, D., "Recent Progress on High-Repetition Rate Laser-Plasma Acceleration," OSA Proceedings, vol. Volume,pp. Pages, Date 2018.

[9] Phuoc, K.T., "Laser based synchrotron radiation," Phys. Plasmas, 12, pp. 023101, 2005.

[10] Albert, F., "Laser Wakefield Accelerators: Next-Generation Light Sources," Optics and Photonics News, 29 (January 2018), pp. 42-49, 2018.

[11] Nemoto, K., "Laser-triggered ion acceleration and table top isotope production," Appl. Phys. Lett., 78, pp. 595-597, 2001.

[12] Spencer, I., "Laser generation of proton beams for the production of short-lived positron emitting radioisotopes," Nucl. Instrum. Meth. B, 183, pp. 449-458, 2001.

[13] Ledingham, K., Bolton, P., Shikazono, N., and Ma, C.M., "Towards Laser Driven Hadron Cancer Radiotherapy: A Review of Progress," Appl. Sci., 4, pp. 402-443, 2014.

[14] Daido, H., Nishiuchi, M., and Pirozhkov, A.S., "Review of laser-driven ion sources and their applications," Reports on Progress in Physics, 75, pp. 056401, 2012.

[15] Macchi, A., Borghesi, M., and Passoni, M., "Ion acceleration by superintense laser-plasma interaction," Rev. Mod. Phys., 85, pp. 751-793, 2013.

[16] Esarey, E., Schroeder, C.B., and Leemans, W.P., "Physics of laser-driven plasma-based electron accelerators," Rev. Mod. Phys., 81, pp. 1229-1285, 2009.

[17] Witte, K., "Physics of ultra-intense laser-plasma interaction," Plasma Physics and Controlled Fusion, 41, pp. B221-B230, 1999.

[18] Salehi, F., "MeV electron acceleration at 1 kHz with <10 mJ laser pulses," Opt Lett, 42, pp. 215-218, 2017.

[19] He, F., "Ponderomotive acceleration of electrons by a tightly focused intense laser beam," Phys. Rev. E, 68, pp. 046407, 2003.

[20] Schmid, K., and Veisz, L., "Supersonic gas jets for laser-plasma experiments," Rev. Sci. Instrum., 83, pp. 053304, 2012.

[21] Sylla, F., Veltcheva, M., Kahaly, S., Flacco, A., and Malka, V., "Development and characterization of very dense submillimetric gas jets for laser-plasma interaction," Rev. Sci. Instrum., 83, pp. 033507, 2012.

[22] Semushin, S., and Malka, V., "High density gas jet nozzle design for laser target production," Rev. Sci. Instrum., 72, pp. 2961-2965, 2001.

[23] Settles, G.S., and Hargather, M.J., "A review of recent developments in schlieren and shadowgraph techniques," Meas. Sci. Technol., 28, pp. 042001, 2017.

[24] Lim, H.D., Wu, J., New, T.H.D., and Shi, S., "Optical Flow Technique for Supersonic Jet Measurements," World Academy of Science, Engineering and Technology, 10, pp. 1228, 2016.

[25] Sang, B.H., and Jeon, T.I., "Pressure-dependent refractive indices of gases by THz time-domain spectroscopy," Opt. Expr., 24, pp. 29040-29047, 2016.

[26] Couperus, J.P., "Tomographic characterisation of gas-jet targets for laser wakefield acceleration," Nucl. Instrum. Meth. A, 830, pp. 504-509, 2016.

[27] Santos, D., "Evaluation of Femtosecond Laser-Induced Breakdown Spectroscopy for Analysis of Animal Tissues," Appl. Spectrosc., 62, pp. 1137-1143, 2008.

[28] Bello, L.T., "Mercury Amalgam Diffusion in Human Teeth Probed Using Femtosecond LIBS," Appl. Spectrosc., 71, pp. 659-669, 2017.

[29] https://physics.nist.gov/PhysRefData/ASD/lines_form.html?, accessed June 2018 Access, 2018

[30] Goers, A.J., Yoon, S.J., Elle, J.A., Hine, G.A., and Milchberg, H.M., "Laser wakefield acceleration of electrons with ionization injection in a pure N^{5+} plasma waveguide," Appl. Phys. Lett., 104, pp. 214105, 2014.